

Travelling fronts in active-passive particle mixtures

Adam Wysocki, Roland G. Winkler, Gerhard Gompper¹

¹*Theoretical Soft Matter and Biophysics, Institute of Complex Systems and Institute for Advanced Simulation, Forschungszentrum Jülich, 52425 Jülich, Germany*

(Dated: March 11, 2022)

The emergent dynamics in phase-separated mixtures of isometric active and passive Brownian particles is studied numerically in two dimensions. A novel steady-state of well-defined traveling fronts is observed, where the interface between the dense and the dilute phase propagates and the bulk of both phases is (nearly) at rest. Two kind of interfaces, advancing and receding, are formed by spontaneous symmetry breaking, induced by an instability of a planar interface due to the formation of localized vortices. The propagation arises due to flux imbalance at the interface, strongly resembling travelling fronts in reaction-diffusion systems. Above a threshold, the interface velocity decreases linearly with increasing fraction of active particles.

PACS numbers: 82.70.Dd, 64.75.Xc

Introduction – Generic models of active fluids divide into two main classes, systems of active Brownian particles (discs or spheres) [1, 2], which emphasize volume exclusion, and systems of anisotropic (or elongated) self-propelled particles, which emphasize alignment interactions, like the Vicsek model [3, 4]. The most striking phenomenon of active Brownian particles (ABPs), observed in various experiments [5–8] and simulations [9–11], is motility-induced phase separation [12]. The phase behavior and kinetics, like domain coarsening [10, 13] or interface fluctuations [14], of ABPs resemble a passive fluid with attractive interaction. Moreover, ABPs exhibit an intriguing collective dynamics with jets and swirls, which has been speculated to arise from interfacial sorting of ABPs with different orientations [11]. In contrast, the kinetics of models with alignment interaction exhibits various modes of collective motion, for example large polar swarms, i.e., high-density polar bands travelling coherently through an isotropic background gas [3, 4].

A natural extension of single-component ABP fluids are mixtures of particles with, e.g., different activities [15–18], temperatures [19, 20], or diameters [21]. These models also exhibit activity-induced phase separation. We focus here on the dynamics of mixtures of isometric active and passive Brownian particles. Surprisingly, we find that these systems exhibit a novel and so far unexplored type of collective motion in the phase-separated state in the form of well-defined propagating fronts, which can be either enriched or depleted of active particles, and are advancing toward or receding from the dense phase, respectively. The propagation arises due to flux imbalance at the interface between the dense and dilute phases with a strong resemblance to travelling fronts in reaction-diffusion systems [22]. The selection of the interface type (advancing or receding) happens by spontaneous symmetry breaking, induced by an instability of a planar interface due to the formation of localized vortices. In contrast to the polar bands of the Vicsek model [3, 4], which travel as a whole, here only the interface

between the two phases propagates.

The recent finding of a stable interface in pure, phase-separated ABP fluids, together with a negative surface tension [14], questions the mapping of an ABP fluid onto an equilibrium fluid with attraction. The emergence of travelling fronts in active-passive mixtures clearly contradicts the existence of an equivalent equilibrium system in this case. Instead, we propose an explanation of the interface dynamics on the basis of well-studied models describing the growth of rough surfaces under far-from-equilibrium conditions [23, 24].

Model – We simulate a mixture of N_A active and N_P passive Brownian disks (in total $N = N_A + N_P$ particles) in a 2D simulation box of size $L_x \times L_y$ with periodic boundary conditions. Their dynamics is overdamped, i.e., $\dot{\mathbf{r}}_i = V_0 \mathbf{e}_i + \mathbf{f}_i/\gamma_t + \boldsymbol{\xi}_i$, where V_0 is the propulsion velocity along the polar axis \mathbf{e}_i ($V_0 = 0$ for passive particles), $\mathbf{f}_i = \sum_{j \neq i} \mathbf{f}_{ij}$ is the force due to steric interactions, and $\boldsymbol{\xi}_i$ is a random velocity. The particles interact via the soft repulsive force $\mathbf{f}_{ij} = k(a_i + a_j - |\mathbf{r}_{ij}|)\mathbf{r}_{ij}/|\mathbf{r}_{ij}|$, with $\mathbf{r}_{ij} = \mathbf{r}_i - \mathbf{r}_j$ if $a_i + a_j < |\mathbf{r}_{ij}|$ and $\mathbf{f}_{ij} = 0$ otherwise [9]. The discs are polydisperse in order to avoid crystallization and their radii a_i are uniformly distributed in the interval $[0.8a, 1.2a]$ [9]. The zero-mean Gaussian white-noise velocity $\boldsymbol{\xi}_i$ obeys $\langle \boldsymbol{\xi}_i(t)\boldsymbol{\xi}_i(t') \rangle = 2D_t \delta_{ij} \mathbf{1} \delta(t - t')$, where $D_t = k_B T/\gamma_t$ is the translational diffusion coefficient with thermal energy $k_B T$ and friction coefficient γ_t . The propulsion direction \mathbf{e}_i undergoes a free rotational diffusion with a diffusion constant D_r , where $D_t/D_r = 4a^2/3$ holds for a no-slip sphere. The persistence of swimming is characterised by the Péclet number $Pe = V_0/(2aD_r)$. The typical particle overlap due to activity, $\gamma_t V_0/(2ak)$, is fixed to 0.01 [13]. Unless otherwise noted, we consider systems with $Pe = 100$ and an packing fraction $\phi = \sum_{i=1}^N \pi a_i^2/(L_x L_y) = 0.67$, below random closed packing [9], and vary the fraction $x_A = N_A/N$ of ABPs. Moreover, lengths are expressed in units of $2a$ and time in units of $1/D_r$.

Phase behavior – A mixture of active and passive discs

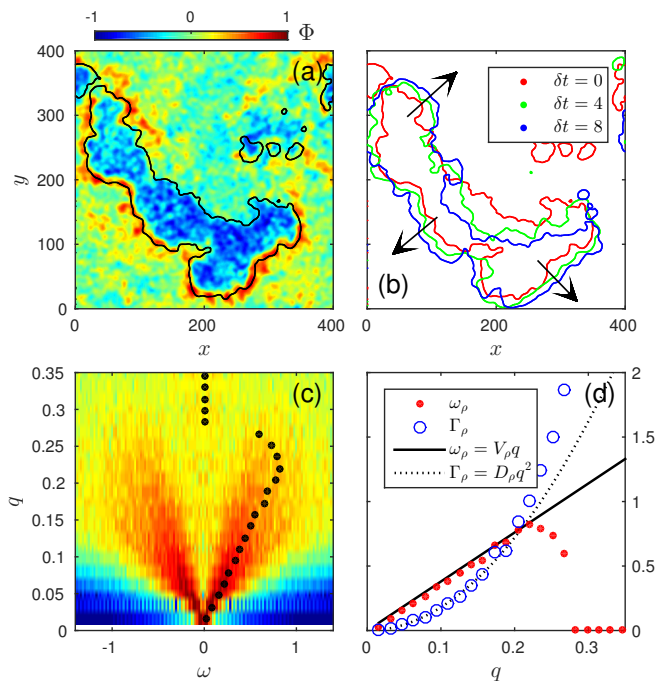


FIG. 1. (color online) (a) Snapshot of the segregation order parameter field $\Phi(\mathbf{r})$ of a system of size $L_x = L_y = 400$ with $N = 160000$ particles ($\phi = 0.78$) in the steady state at $x_A = 0.5$. $\Phi = 1$ ($\Phi = -1$) corresponds to a pure active (passive) phase and $\Phi = 0$ corresponds to a uniform mixture. The black line indicates the interface position. (b) Time evolution of the interface position, see movies in [25]. (c) Dynamic structure factor $S(\omega, q)$ as a function of frequency ω and wavenumber q . The shape of $S(\omega, q)$ indicates a damped propagative mode. (d) Frequency ω_ρ (also indicated in (c) by black dots) and damping rate Γ_ρ as function of wavenumber. Lines indicate $\omega_\rho = V_\rho q$, with $V_\rho \approx 0.04V_0$, and $\Gamma_\rho = D_\rho q^2$, with $D_\rho \approx 0.004D_0$, where D_0 is the diffusion constant of a free ABP.

separates into a dense and a dilute phase at sufficiently large Pe , ϕ , and x_A [16], very similar to a pure ABP fluid [10]; in addition, active and passive particles tend to segregate inside the dense phase. This is illustrated in Fig. 1(a), where the segregation order parameter field $\Phi(\mathbf{r})$ of a large phase-separated system with curved interfaces between the dense and the dilute phase is shown. Φ is defined as $\Phi(\mathbf{r}) = (\phi_A - \phi_P)/(\phi_A + \phi_P)$ with coarse-grained packing density fields $\phi_A(\mathbf{r})$ and $\phi_P(\mathbf{r})$ of active and passive particles, respectively [25]. The dilute phase consist mainly of passive particles ($\Phi \approx -1$) and the bulk of the dense phase is a homogenous active-passive mixture ($\Phi \approx 0$) with small patches of enriched active or passive particles. Within the interface region, we observe either an accumulation ($\Phi \approx 1$) or a depletion ($\Phi < 0$) of active particles.

Note that a completely different behavior appears for dilute solutions (not considered here), namely, for mean free paths much larger than the persistence length of swimming ($\pi\sigma/4\phi \gg V_0/D_r$), where active (passive) par-

ticles behave as effectively 'hot' ('cold') particles. Such a mixture exhibits phase separation into a solid-like cluster of passive and a gaseous phase of the active particles [20].

Bulk travelling fronts – The focus of our paper is on the kinetics of a phase-separated active-passive mixture. The domain dynamics of a one-component ABP fluid in the steady state is limited to fluctuating interfaces resembling thermal capillary waves [14, 25], except for the coarsening kinetics [10, 13]. By contrast, active-passive mixtures exhibit amazingly mobile or travelling interfaces in a large region of the $Pe - \phi - x_A$ parameter space. The interface propagation becomes apparent from Fig. 1(b), where the time evolution of the interface position is shown, see also movies in Ref. [25].

In order to quantify our observations, we analyse the density correlations at $x_A = 0.5$ and $\phi = 0.78$ by the dynamic structure factor $S(\mathbf{q}, \omega) = \int_{-\infty}^{\infty} F(\mathbf{q}, t) \exp(i\omega t) dt$, where \mathbf{q} is the wavevector, ω is the angular frequency, and $F(\mathbf{q}, t) = \langle \rho_{\mathbf{q}}(t) \rho_{-\mathbf{q}}(0) \rangle / N$ is the correlation function of the Fourier components $\rho_{\mathbf{q}}$ of the density [26]. The circularly averaged $S(\mathbf{q}, \omega)$, which is accessible by scattering experiments, is shown in Fig. 1(c). The structure factor exhibits peaks at the frequencies $\pm\omega_\rho$, with a width, which increases with increasing q . This suggests a damped propagative mode [26] related to the traveling interfaces indicated in Fig. 1(b). We obtain the full dispersion relations $\omega_\rho(q)$ and $\Gamma_\rho(q)$ by fitting $F(q, 0) \exp(-\Gamma_\rho t) \cos(\omega_\rho t)$ to the corresponding simulation data. As can be seen in Fig. 1(d), the peak positions follow the Brillouin-like dispersion relation $\omega_\rho = V_\rho q$ up to $q \approx 0.2$ with a velocity $V_\rho \approx 0.04V_0$. In a simple equilibrium fluid (Newtonian dynamics) such a velocity is the speed of sound [26], but here, V_ρ is related to the velocity of interface propagation. The decay rate $\Gamma_\rho(q)$ obeys $\Gamma_\rho = D_\rho q^2$ up to $q \approx 0.2$, with the transport coefficient $D_\rho \approx 0.004D_0$, where $D_0 = D_t + V_0^2/(2D_r)$ is the diffusion constant of a free ABP. All modes are strongly damped for $q > 0.25$, i.e. dense (or dilute) phase droplets with size smaller than $50a$ dissolve quickly.

Stabilized travelling fronts – In order to study a propagating interface in more detail, we employ a quasi-one-dimensional setup of an elongated box of lengths $L_x = 2L_y$ [14, 27] such that the interface favors to span the shorter box length, see Fig. 2(a). Given that the system phase-separates, such a configuration forms spontaneously and remains stable over long time. In Fig. 3 (a,b), we show the time evolution of the active-particle packing profile $\phi_A(x, t)$ averaged over the y -coordinate. The interface position in a pure active fluid performs a diffusive motion [25]. By contrast, in our mixture the translational symmetry is broken and both interfaces propagate steadily in parallel (for the set up of Fig. 2) either to the right or to the left with equal probability [25]. The travelling front is extremely stable within the typical simulation length of $T = 5 \times 10^3$, however, the steady propagation is occasionally interrupted by in-

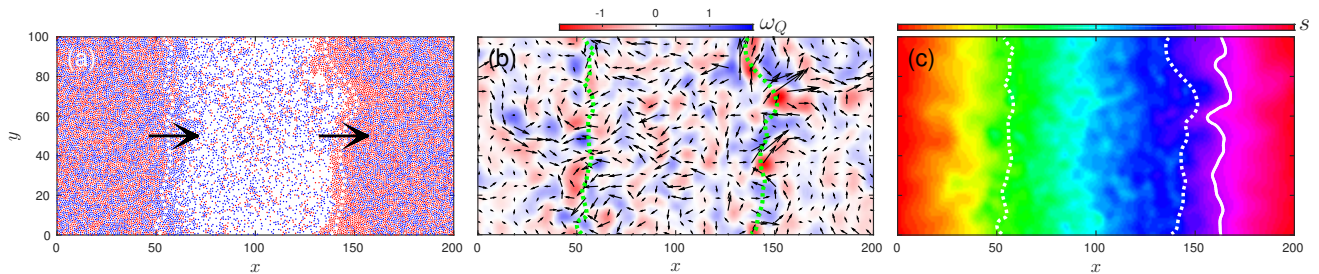


FIG. 2. (color online) (a) Snapshot of a mixture of active (red) and passive (blue) Brownian discs at $x_A = 0.5$ in a box of size $L_x = L_y/2 = 100$. The interfaces between the two phases (dashed lines) travel by chance to the right. (b) Vorticity $\omega_Q(\mathbf{r}) = \nabla \times \mathbf{Q}(\mathbf{r})$, where \mathbf{Q} is the coarse-grained particle flux [25]. (c) Visualisation of the bulk flow. Particle positions are shown after the time lag $\delta t = 2$, where particles are colored according to their initial x position, as indicated by the color scale. The solid line marks the isoline of $s(\mathbf{r}, \delta t)$ used for the stability analysis. See corresponding movies in Ref. [25].

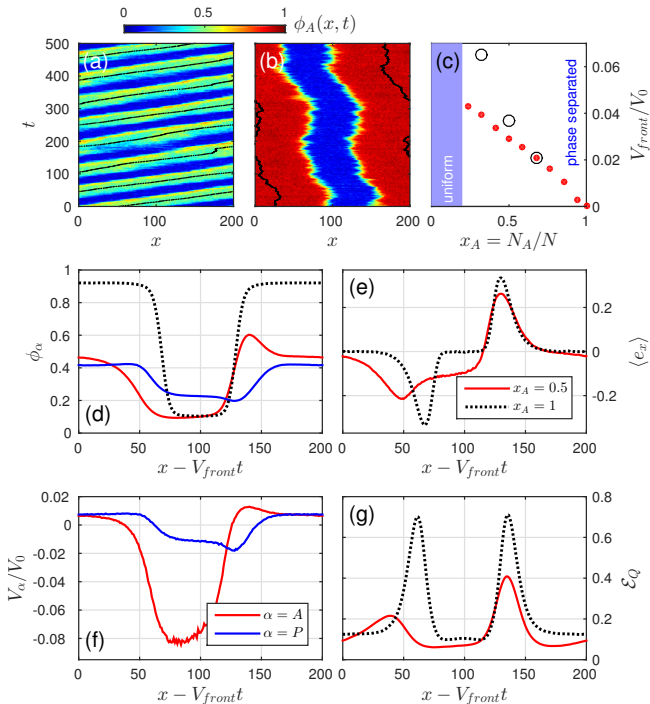


FIG. 3. (color online) Space-time dependence of the active-particle packing density $\phi_A(x, t)$ for (a) the mixture with $x_A = 0.5$ and (b) a pure active fluid with $x_A = 1$. The black lines indicate the center-of-mass position of $\phi_A(x, t)$. (c) Velocities V_{front} (bullets) of the interface and V_ρ (circles) extracted from $S(q, \omega)$, see Fig. 1, as function of x_A . Phase separation appears for $x_A = 0.2$. (d-g) Time averaged profiles measured in a comoving frame, i.e., relative to the propagating front, (d) of active- and passive-particle packing fractions $\phi_A(x)$ and $\phi_P(x)$, (e) of the active-particle x -polarisation $\langle e_x \rangle(x)$, (f) of active- and passive-particle velocities along the front propagation direction $V_A(x)$ and $V_P(x)$, and (g) of the intensity of the particle flux vorticity $\mathcal{E}_Q(x)$. We choose a representation, where the front propagates to the right. Solid lines correspond to $x_A = 0.5$ and dashed lines to $x_A = 1$.

termittent large-scale rearrangements of the front. The front velocity V_{front} is nearly independent of the over-

all packing fraction ϕ and activity Pe . However, V_{front} monotonously decreases with increasing x_A [in a good agreement with V_ρ obtained from $S(q, \omega)$], with a maximum just above the active-particle fraction, where phase separation sets in, see Fig. 3 (c).

We calculate profiles of various quantities in a comoving frame. In a pure active fluid, the two interfaces are equivalent and the dense phase is symmetrically surrounded by a corona of particles with their polar vector pointing preferentially toward that phase, see dashed lines in Fig. 3(d,e). In a mixture, this symmetry is broken and active particles preferentially accumulate at one interface and deplete at the other. Similarly, the x -polarisation $\langle e_x \rangle$ at both interfaces is different; it is larger at the side of preferred accumulation. Moreover, $\langle e_x \rangle$ takes negative values in the dilute phase, accompanied by a negative x -velocity of active particles, V_A , causing in turn a negative velocity of passive particles, V_P , due to collisions between passive and active particles, see Fig. 3(f). The mass transport from the dense into the dilute phase is characterized by the intensity of the particle flux vorticity $\mathcal{E}_Q(x) = \int_0^{L_y} \omega_Q^2(\mathbf{r}) dy / L_y$ (see detailed discussion below), where $\omega_Q(\mathbf{r})$ is the curl of the particle flux $\mathbf{Q}(\mathbf{r})$. \mathcal{E}_Q is most pronounced within the interface region and, in case of a mixture, \mathcal{E}_Q is larger at the side of larger polarisation and active particle accumulation, see Fig. 3(g) and Fig. 2(b).

Discussion of interfaces in pure ABP fluids – Interfaces in pure ABP fluids are not propagating, but show a diffusive dynamics as evident from Fig. 3(b) and the movies in Ref. [25]. Within the picture of motility-induced phase separation, there is a balance between an active flux of particles from the low-density gas phase colliding with the dense phase and a diffusive flux of particles leaving the high-density phase due to rotational diffusion [10]. This alone would generate a very rough and uncorrelated interface structure, like in random particle deposition [23].

However, activity also leads to smoothing of the interface. For an undulated interface, particles which bump

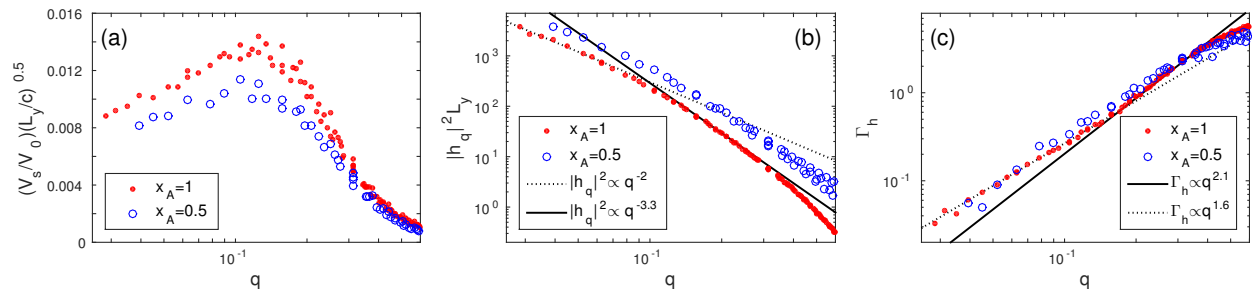


FIG. 4. (color online) (a) Growth velocities $V_s(q)$ of the Fourier modes of an isoline of the scalar displacement field $s(\mathbf{r}, \delta t)$ inside the dense phase, see Fig. 2(c). (b) Spectrum of the interfacial height fluctuations $\langle |h_q|^2 \rangle$ as a function of the wave number q ; results for different L_y at fixed L_y/L_x are shown. (c) Decay rate $\Gamma_h(q)$ of the interfacial height autocorrelation function $\langle h_q(t)h_{-q}(0) \rangle$. Different scaling regimes are indicated by lines.

into the interface slide into regions of high convexity [11, 28], thereby level out the interface on small scales and produce a local polarisation. In turn, this local polarisation induces an internal mass flow inside the dense phase such that alternating vortices of opposite vorticity emerge within the interface region due to mass conservation, see Fig. 3(g) and movies in Ref. [25]. As a result, randomly oriented particles emerge from the bulk and cause an evaporation of the interface protrusions.

Discussion of interfaces in active-passive mixtures –

This picture changes considerably in mixtures, where the interfaces are propagating due to the dynamical coupling of active and passive particles. Imagine a perturbation such that the polarisation in the right interface region of Fig. 2(a) is larger than that in the left one. Hence, more active particles leave the right interface, due to a larger vorticity, and the collision-induced flux of passive particles from right to left exceeds the opposite flux. Now, a corona of passive particles covers the dense phase in the left interface region and inhibits the further discharge of active particles. This is supported by the shape of the profiles $\phi_A(x)$, $\phi_P(x)$, $\langle e_x \rangle(x)$, and $\mathcal{E}_Q(x)$ in Fig. 3. The overall picture that the traveling front is a consequence of a flux imbalance and that the particle transport out of the interface is dominated by vortex formation and not by rotational diffusion is in line with the fact that V_{front} is independent of Pe , if V_0 is fixed and D_r is varied via $k_B T$. In order to quantify the vorticity-induced mass transport, we use the horizontal positions $x_i(t)$ of all particles i (at time t) to construct a scalar displacement field $s(\mathbf{r}, \delta t)$ [25]. The temporal evolution of $s(\mathbf{r}, \delta t)$ then indicates the particle convection, see Fig. 2(c) and movies in Ref. [25]. We choose a isoline of $s(\mathbf{r}, \delta t)$ inside the dense phase; this isoline is initially flat, but roughens as a function of time. This process is monitored by the Fourier modes of this isoline, similar to a stability analysis of the Rayleigh-Taylor instability. The Fourier-mode amplitudes grow with constant velocity $V_s(q)$ at short times. The growth velocities first increase with increasing q , reach a maximum at $q \approx 0.1$, and exhibit a fast

decay for larger q , see Fig. 4(a). This confirms the visual impression in Fig. 2(b,c) of a characteristic length scale of internal mass currents.

Interface correlations and relaxation – We analyse the structure and dynamics of the interface by a Fourier transform of its fluctuations. From the Fourier amplitudes h_q [25], we obtain the interface structure factor $S(q) = \langle |h_q|^2 \rangle$ and the autocorrelation function $\langle h_q(t)h_{-q}(0) \rangle$, which we fit by $S(q) \exp(-\Gamma_h t)$ to obtain the damping rate $\Gamma_h(q)$ as function of q . We observe a length-scale-dependent scaling $S \propto q^{-(1+2\alpha)}$ and $\Gamma_h \propto q^z$, where α and z are the roughness and the dynamic exponent, respectively [29]. We find $\alpha \approx 1/2$ and $z \approx 1.6$ on large scales, $q \lesssim 0.1$, and $\alpha \approx 1$ and $z \approx 2$ on intermediate scales, $0.1 \lesssim q \lesssim 0.4$, for static as well as traveling interfaces, see Fig. 4(b,c). In comparison, an overdamped fluid interface with thermally excited capillary waves in equilibrium has $\alpha = 1/2$ [27] and $z = 1$ [30] for $q < 0.6$. However, physically more related is the Edward-Wilkinson model [23, 24], for non-equilibrium interface growth – where random particle arrival leads to interface roughening, while lateral motion (e.g., due to gravity) yields interface smoothing – with exponents $\alpha = 1/2$ and $z = 2$. If additionally local growth perpendicular to the interface is present, as in the Kardar-Parisi-Zhang model, the dynamic exponent $z = 3/2$ is expected [23, 24], very close to the exponents characterizing the interface behavior of our active particle fluids.

Conclusions – Active-particle systems display many unexpected features – both static and dynamic. We have shown that the large-scale interface structure in mixtures is similar to that at equilibrium, however, the dynamics, like interface relaxation or front propagation, exhibits strong nonequilibrium characteristics. Our results call for an experimental investigation over a wide range of concentrations and activities. Active-passive mixtures could be realized experimentally by active colloids [5–8], vibrated polar disks [31] or even robots [32, 33].

We thank A. Varghese and J. Horbach for helpful discussions. The support by the DFG priority pro-

gram SPP1726 on “Microswimmers” is gratefully acknowledged.

-
- [1] J Elgeti, R G Winkler, and G Gompper, “Physics of microswimmers—single particle motion and collective behavior: a review,” *Rep. Prog. Phys.* **78**, 056601 (2015).
- [2] M Cristina Marchetti, Yaouen Fily, Silke Henkes, Adam Patch, and David Yllanes, “Structure and mechanics of active colloids,” arXiv:1510.00425 (2015).
- [3] Guillaume Grégoire and Hugues Chaté, “Onset of collective and cohesive motion,” *Phys. Rev. Lett.* **92**, 025702 (2004).
- [4] Alexandre P. Solon, Hugues Chaté, and Julien Tailleur, “From phase to microphase separation in flocking models: The essential role of nonequilibrium fluctuations,” *Phys. Rev. Lett.* **114**, 068101 (2015).
- [5] I. Theurkauff, C. Cottin-Bizonne, J. Palacci, C. Ybert, and L. Bocquet, “Dynamic clustering in active colloidal suspensions with chemical signaling,” *Phys. Rev. Lett.* **108**, 268303 (2012).
- [6] Jeremie Palacci, Stefano Sacanna, Asher Preska Steinberg, David J. Pine, and Paul M. Chaikin, “Living crystals of light-activated colloidal surfers,” *Science* **339**, 936–940 (2013).
- [7] Ivo Buttinoni, Julian Bialké, Felix Kümmel, Hartmut Löwen, Clemens Bechinger, and Thomas Speck, “Dynamical clustering and phase separation in suspensions of self-propelled colloidal particles,” *Phys. Rev. Lett.* **110**, 238301 (2013).
- [8] Félix Ginot, Isaac Theurkauff, Demian Levis, Christophe Ybert, Lydéric Bocquet, Ludovic Berthier, and Cécile Cottin-Bizonne, “Nonequilibrium equation of state in suspensions of active colloids,” *Phys. Rev. X* **5**, 011004 (2015).
- [9] Yaouen Fily, Silke Henkes, and M. Cristina Marchetti, “Freezing and phase separation of self-propelled disks,” *Soft Matter* **10**, 2132–2140 (2014).
- [10] Gabriel S. Redner, Michael F. Hagan, and Aparna Baskaran, “Structure and dynamics of a phase-separating active colloidal fluid,” *Phys. Rev. Lett.* **110**, 055701 (2013).
- [11] Adam Wysocki, Roland G. Winkler, and Gerhard Gompper, “Cooperative motion of active brownian spheres in three-dimensional dense suspensions,” *Europhys. Lett.* **105**, 48004 (2014).
- [12] Michael E. Cates and Julien Tailleur, “Motility-induced phase separation,” *Annu. Rev. Condens. Matter Phys.* **6**, 219–244 (2015).
- [13] Joakim Stenhammar, Davide Marenduzzo, Rosalind J. Allen, and Michael E. Cates, “Phase behaviour of active brownian particles: the role of dimensionality,” *Soft Matter* **10**, 1489–1499 (2014).
- [14] Julian Bialké, Jonathan T. Siebert, Hartmut Löwen, and Thomas Speck, “Negative interfacial tension in phase-separated active brownian particles,” *Phys. Rev. Lett.* **115**, 098301 (2015).
- [15] Ran Ni, Martien A. Cohen Stuart, Marjolein Dijkstra, and Peter G. Bolhuis, “Crystallizing hard-sphere glasses by doping with active particles,” *Soft Matter* **10**, 6609–6613 (2014).
- [16] Joakim Stenhammar, Raphael Wittkowski, Davide Marenduzzo, and Michael E. Cates, “Activity-induced phase separation and self-assembly in mixtures of active and passive particles,” *Phys. Rev. Lett.* **114**, 018301 (2015).
- [17] Felix Kummel, Parmida Shabestari, Celia Lozano, Giovanni Volpe, and Clemens Bechinger, “Formation, compression and surface melting of colloidal clusters by active particles,” *Soft Matter* **11**, 6187–6191 (2015).
- [18] Sho C. Takatori and John F. Brady, “A theory for the phase behavior of mixtures of active particles,” *Soft Matter* **11**, 7920–7931 (2015).
- [19] A. Y. Grosberg and J.-F. Joanny, “Nonequilibrium statistical mechanics of mixtures of particles in contact with different thermostats,” *Phys. Rev. E* **92**, 032118 (2015).
- [20] Simon N Weber, Christoph A Weber, and Erwin Frey, “Binary mixtures of particles with different diffusivities demix,” arXiv:1505.00525 (2015).
- [21] Xingbo Yang, M. Lisa Manning, and M. Cristina Marchetti, “Aggregation and segregation of confined active particles,” *Soft Matter* **10**, 6477–6484 (2014).
- [22] John J. Tyson and James P. Keener, “Singular perturbation theory of traveling waves in excitable media (a review),” *Physica D* **32**, 327 – 361 (1988).
- [23] A.L. Barabási and H.E. Stanley, *Fractal Concepts in Surface Growth* (Cambridge University Press, 1995).
- [24] Joachim Krug, “Origins of scale invariance in growth processes,” *Adv. Phys.* **46**, 139–282 (1997).
- [25] See the Supplemental Material at XXX for movies corresponding to Fig. 1(a,b) and Fig. 2 and for analogous movies of a pure ABP fluid. Details on the definition of coarse-grained fields and interface position are provided.
- [26] J.P. Hansen and I.R. McDonald, *Theory of Simple Liquids* (Elsevier Science, 1990).
- [27] R. L. C. Vink, J. Horbach, and K. Binder, “Capillary waves in a colloid-polymer interface,” *J. Chem. Phys.* **122**, 134905 (2005).
- [28] Yaouen Fily, Aparna Baskaran, and Michael F. Hagan, “Dynamics of self-propelled particles under strong confinement,” *Soft Matter* **10**, 5609–5617 (2014).
- [29] Martin Siegert, “Determining exponents in models of kinetic surface roughening,” *Phys. Rev. E* **53**, 3209–3214 (1996).
- [30] Markus Gross and Fathollah Varnik, “Interfacial roughening in nonideal fluids: Dynamic scaling in the weak- and strong-damping regime,” *Phys. Rev. E* **87**, 022407 (2013).
- [31] Julien Deseigne, Olivier Dauchot, and Hugues Chaté, “Collective motion of vibrated polar disks,” *Phys. Rev. Lett.* **105**, 098001 (2010).
- [32] Michael Rubenstein, Alejandro Cornejo, and Radhika Nagpal, “Programmable self-assembly in a thousand-robot swarm,” *Science* **345**, 795–799 (2014).
- [33] Mite Mijalkov, Austin McDaniel, Jan Wehr, and Giovanni Volpe, “Engineering sensorial delay to control phototaxis and emergent collective behaviors,” arXiv:1511.04528 (2015).